Elastic and mechanical studies of the transition in LaP_5O_{14}: A continuous ferroelastic transition with a classical Landau-type behavior

Gilles Errandonea
Centre National d'Etudes des Télécommunications, 196 rue de Paris, 92220 Bagneux, France
(Received 6 August 1979)

We report a detailed experimental checking of the phenomenological Landau theory of phase transitions applied to a structural transition involving a homogeneous deformation (ferroelastic transition). We have determined the temperature dependence of 17 physical quantities on both sides of the ferroelastic transition ($mmm \rightarrow 2/m$; $T_c = 125\,^{\circ}C$) of lanthanum pentaphosphate (LaP_5O_{14}). At each temperature, the thermal-strain-tensor components have been measured by mechanical dilatometry and accurate γ-ray diffractometry, and the 13 components of the elastic-stiffness tensor have been deduced from Brillouin-scattering measurements performed in seven scattering configurations. The thermal-expansion coefficients are discontinuous at T_c while the monoclinic shear c_5 continuously vanishes with the classical critical exponent $\beta = 0.500 \pm 0.007$. The associated elastic constant c_{55} is also found to vanish at T_c with the exponents $\gamma = \gamma' = 1.00 \pm 0.02$ in relation with the occurrence of a soft transverse-acoustic mode. The temperature dependence of all the measured quantities is accounted for in the framework of the Landau theory using a free-energy expansion truncated at the fourth-order terms. The ferroelastic transition is assumed to be driven by the softening of a B_{2g} soft optic mode whose normal coordinate is strongly and linearly coupled with c_5. This coordinate is also quadratically coupled with the diagonal components of the strain tensor. Thus the set of our experimental data can be satisfactorily fitted with only four coupling coefficients. Furthermore, this model can be quantitatively extended to the other isomorphous ferroelastic rare-earth pentaphosphates, and it predicts correctly the jump of the specific heat at T_c and the pressure dependence of the soft-optic-mode frequency in good agreement with the available experimental data. Finally, the introduction of some corrective terms is discussed.

I. INTRODUCTION

It is well known that ferroelastic phase transitions induce anomalies in the elastic and mechanical properties of a crystal.[1-4] The mean-field Landau theory of phase transitions[1-5] is the simplest theory to account for these anomalies. However, in general, this classical theory is not valid near the transition when the influence of the fluctuations is not negligible.[6]

More precisely, one has to distinguish whether or not the spontaneous strain occurring in the ferroelastic phase has the same symmetry as the order parameter associated with the transition.[1-4] In the latter case, the transition is "improper"[2] and has to be studied in the frame of the more sophisticated renormalization-group theory when one is interested in the critical behavior of the material in the neighborhood of the transition.

The former case corresponds to "proper"[2] ferroelastic materials and is quite different. Actually, Cowley[7] and Schwabl[7] have demonstrated that, for second-order or weak first-order proper ferroelastic transitions, the Landau theory is strictly valid except in a few cases where one must include logarithmic corrections. These cases arise when the wave vectors of the strongly temperature-dependent acoustic modes lie within planes of the reciprocal space instead of having particular directions.

However, up to now, we lack complete experimental data in both the ferroelastic and paraelastic phase to verify the consequences of the Landau theory on the whole set of mechanical and elastic properties of a ferroelastic material. Rare-earth pentaphosphates, ReP_5O_{14} (with Re = La to Tb), are ideal materials to make such a verification since they belong to the simplest class of ferroelastic materials: they undergo a pure second-order ferroelastic transition of the proper type, having a one-dimensional order parameter without any change of the translational symmetry.[8,9] Besides, the low symmetry ($2/m$) of the ferroelastic phase allows one to test the Landau theory for a large number of physical quantities (13 different components of the elastic-stiffness tensor and 4 of the thermal-strain tensor). Finally, the accessibility of the transition temperature [from $T_c = 125\,^{\circ}C$ for LaP_5O_{14} to $174\,^{\circ}C$ for TbP_5O_{14} (Refs. 8–10)] and the high crystalline and optical quality of the available samples of LaP_5O_{14} and NdP_5O_{14} (typical volume 1 cm^3) provide good experimental opportunities for this study in contrast with other proper second-order ferroelastic materials like $DyVO_4$

($T_c = -259\,°C$),[11] $LiNH_4C_4H_4O_6 \cdot H_2O$ ($T_c = -175\,°C$),[12] $KH_3(SeO_3)_2$ ($T_c = -62\,°C$),[13] and TeO_2 (pressure-induced transition).[14]

Several workers have been interested in the exceptional fluorescence properties[15] of NdP_5O_{14} upon which are based miniature laser devices.[16,17] Their studies led to the discovery of ferroelastic properties in this material and in isostructural compounds. Budin[9] and Weber *et al.*[9] have described the very mobile and switchable domain structure of NdP_5O_{14} and $La_{0.25}Nd_{0.75}O_{14}$. Crystallographic measurements[8] have shown that the space-group change is from *Pncm* (conventional setting *Pmna*) above T_c to $P2_1/c$. Below T_c, a spontaneous monoclinic shear, e_5, appears in the xz plane with no modification of the number of atoms in the unit cell. Its temperature dependence has been determined by optical measurements.[9] The magnitude of e_5 is approximately 10^{-2} rad at room temperature.

Several soft modes have been observed in these materials. Brillouin-scattering measurements have shown a strong decrease of the sound velocity ($\simeq 170$ m/s) of a transverse-acoustic mode at T_c in LaP_5O_{14} (Ref. 18) and $La_{0.5}Nd_{0.5}P_5O_{14}$ (Ref. 19) demonstrating that the order parameter for the transition belongs to the B_{2g} representation of the *mmm* prototype point group. Besides, a strong softening of two optic modes of B_{2g} and B_{3g} symmetry has also been studied by Raman scattering in LaP_5O_{14},[20,21] NdP_5O_{14},[20,22] and TbP_5O_{14}.[23] Since the softer optic mode has the same B_{2g} symmetry as the e_5 shear, it couples linearly with it, and its softening is believed to induce the ferroelastic transition according to a mechanism described by Miller and Axe.[24,25] Also, the temperature dependences of the spontaneous birefringence in LaP_5O_{14} and $La_{0.25}Nd_{0.75}P_5O_{14}$ (Ref. 26) and of the specific heat in NdP_5O_{14} and PrP_5O_{14} (Ref. 27) have recently been investigated. Finally, the pressure dependence of the soft-optic-mode frequencies has been determined.[28]

In this paper, we are particularly interested in the LaP_5O_{14} compound chosen as the prototype of the ferroelastic rare-earth pentaphosphates. We have measured the temperature dependence of all the components of its thermal-strain and elastic-stiffness tensors in both phases. We have determined the spontaneous shear by γ-ray diffractometry between 20 °C and T_c, the expansion coefficients by mechanical dilatometry between -180 and 220 °C (the expansion coefficients of NdP_5O_{14} were also measured) and the elastic constants from Brillouin-scattering measurements between 20 and 200 °C. The experimental procedures are described in Sec. II and our results are given in Sec. III. In the fourth part of this paper, we present a phenomenological model based on Landau's theory of phase transitions. This model is fitted quantitatively to our measurements as well as to the other available data.

II. EXPERIMENTAL PROCEDURES

All the crystals used in the experiments described below were obtained from a flux-growth technique.[29] As-grown crystals had a typical size of 1 cm^3 and exhibited large high-optical-quality zones. Their mosaic spread determined by γ-ray diffraction was of the order of 10″ they were x-ray oriented and then polished. The misorientation of the polished samples with respect to the required crystallographical orientations was less than 1′ and always negligible for our measurements. They all exhibited the a-type domain structure described by Weber *et al.*[9]

A. Dilatometric measurements

When the undeformed state of the crystal is considered at the transition temperature, the thermal-strain tensor appearing in a free LaP_5O_{14} crystal takes the following form (using the Voigt notation[30]) in the monoclinic phase:

$$\begin{pmatrix} e_1 & 0 & \frac{1}{2}e_5 \\ 0 & e_2 & 0 \\ \frac{1}{2}e_5 & 0 & e_3 \end{pmatrix}, \tag{1}$$

in a frame of reference constituted by the three crystallographic orthorhombic axes.

The e_5 component corresponds to the spontaneous monoclinic shear and vanishes by symmetry in the orthorhombic phase. It transforms according to the B_{2g} representation of the *mmm* point group which induces the ferroelastic transition. Thus, its sign changes from one domain to another.[1,3] Its temperature dependence was measured using a γ-ray-diffractometry apparatus.

Diagonal terms of Eq. (1) represent expansions along the three orthogonal axes of the prototype phase. Since they transform like the totally symmetric A_g representation of *mmm*, they take the same value for the two types of domains of the ferroelastic phase. They were deduced from classical dilatometric measurements.

For the γ-ray measurements we used the LI3 experimental setup of the Laue-Langevin Institute which has already been described by Schneider *et al.*[31] We looked at the (002) Bragg reflection of samples excited by a well-collimated γ line. This reflection splits into two parts in the ferroelastic phase because of the existence of two types of domains. Thus, the angular separation of the two families of reflecting planes gave a measurement of the monoclinic shear e_5.

The excitation line was the 412-keV ($\lambda = 0.03$ Å) radiation from radioactive gold with $\Delta\lambda/\lambda = 10^{-6}$ at room temperature. Its divergence in the scattering

plane was 30″. Measurements have been made on two polydomain samples: The first one was a $3 \times 3 \times 5$ mm^3 rectangular parallelepiped with polished faces perpendicular to the crystallographic axes, and the second one was an as-grown crystal of size $\approx 5 \times 5 \times 8$ mm^3. The temperature of these samples was regulated with a stability of ± 0.01 °C during the time necessary (20′) to measure the spontaneous shear. Rocking curves were recorded by rotating the sample by steps of 4″ through the range of angles where Bragg reflections took place. The instrumental width of the peaks, determined by the divergence of the γ beam, was equal to 30″. Since the peaks were always clearly symmetrical, their angular separation (which is twice the spontaneous shear angle e_5) was measured with an accuracy of $\pm 8''$ (4×10^{-5} rad).

The linear-expansion coefficient of LaP_5O_{14} and NdP_5O_{14} compounds along the crystallographic axes were measured by a standard dilatometric method with a 942 TMA Dupont de Nemours dilatometer between -170 and 370 °C.

Typical sizes of the crystals used were $4 \times 4 \times 9$ mm^3 with the largest dimension corresponding to the measured expansion coefficient. For each direction, measurements were made on several polydomain samples whose horizontal faces were polished but also on as-grown crystals. It appears that the very mobile domain structure does not perturb the results even for the [100] direction for which a surface relief pattern is visible on the faces, since our results on a given sample or on different ones were reproducible within 5%. The heating rate was varied from 0.2 to 2 °C/min, with no significant change in the results.

B. Brillouin-scattering measurements

The temperature dependence of the entire set of the elastic-stiffness-tensor components was deduced from sound-velocity measurements in LaP_5O_{14} between 20 and 200 °C making use of a Brillouin setup.

The main features of a Brillouin-scattering experiment have already been described.[32,33] In our setup, the excitation was provided by a 100-mW He-Ne laser emitting in a single transverse mode at 6328 Å. The incident beam, whose polarization could be rotated with a $\frac{1}{2}\lambda$ plate, was then focused on the sample. The width of the useful scattering volume was about 150 μm. In a few cases, to improve the relative accuracy, sound velocities related to perpendicular directions were simultaneously measured using a 10-cm-focal-length spherical mirror which reflected the beam emerging from the sample. Thus, the sample could be excited by two coincident collinear beams propagating in opposite directions.[34]

The scattered light was analyzed at right angles with a pressure scanned, plane, Fabry-Perot interferometer of free spectral range 1.45 cm^{-1}. This device was used either in a two-pass or in a three-pass configuration.[33] The finesse was, respectively, 60 or 80 and the measured contrast 10^5 or 2×10^6.

The instrumental linewidth was usually 1 GHz, essentially determined by the linewidth of the laser line. It could be reduced by making use of a longitudinal mode selector inserted in the laser cavity. Thus, we obtained a 0.6-GHz instrumental linewidth with the three-pass device, the laser power being reduced to 40 mW.

Some checking, especially for the weakest Brillouin lines, were performed with a CR8 single-mode argon laser emitting at 5145 Å with 1-W power and another Fabry-Perot interferometer whose free spectral range was 1.66 cm^{-1}, contrast 8×10^5, and finesse 90 when used in a three-pass setup, leading also to a 0.6-GHz instrumental linewidth. As a consequence, all the observed Brillouin shifts were measured with an accuracy of about 100 MHz ($\sim 3 \times 10^{-3}$ cm^{-1}).

Samples were heated in a silver furnace provided with four apertures in the directions of the exciting and analyzed beams. The temperature was regulated with a stability of 0.1 °C ($\Delta T/T \approx 3 \times 10^{-4}$). Sample heating by the laser beam was found to be negligible since the transition temperature was reproducible within 0.1 °C on lowering the laser power from 100 to 40 mW.

To determine all the components of the elastic-stiffness tensor, we measured the sound velocities propagating along the crystallographic axes and the bisectors of these axes (i.e., [100], [110], and similar directions). We used several rectangular parallelepiped-shaped polydomain crystals of approximate size $3 \times 3 \times 5$ mm^3 with two typical scattering geometries shown in Fig. 1. For most of the geometries studied, the two different orientations of the sound-propagation directions related to the two types of domains are nearly equivalent since the directions of the monoclinic crystallographic axes only vary slightly from one domain to another.[9]

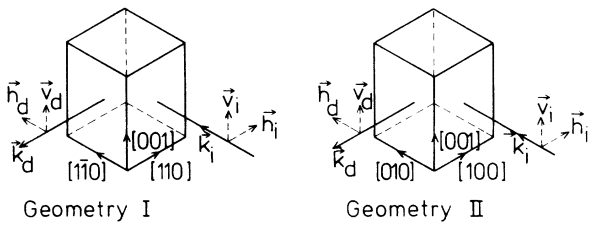

FIG. 1. Typical Brillouin-scattering geometries. $\vec{k}_i$ and $\vec{k}_d$ are the wave vectors of the incident and scattered light, $\vec{v}_i$, $\vec{h}_i$, $\vec{v}_d$, $\vec{h}_d$ their polarizations. We measured the sound velocities along the [100] (geometry I), [110] (geometry II), and all similar directions obtained by permutation of the coordinates.

Thus, the appearance of the spectra was the same whether the scattering volume contained both types of domains or only one. Exceptions were the nonequivalent [101] and [10$\bar{1}$] directions leading to significantly different spectra which we sometimes observed simultaneously in polydomain crystals.

Sound velocities v were deduced from Brillouin shifts $\Delta\nu$ using:

$$v = c\left(\frac{\Delta\nu}{\nu_i}\right)(n_i^2 + n_s^2 - 2n_i n_s \cos\theta)^{-1/2} \quad , \tag{2}$$

where ν_i is the frequency of the incident light, c is the light velocity *in vacuo*, n_i and n_s are, respectively, the refractive indices for the incident and scattered light, and θ is the scattering angle (here $\theta = 90°$).

Refractive indices were measured at room temperature using an Abbe refractometer at 6328 Å. We found $n_x = 1.604$, $n_y = 1.598$, and $n_z = 1.620$. They can be considered as principal indices since at 20 °C the principal axes of the optical indicatrix make an angle of only 8.2° with the crystallographic axes.[26] Their temperature dependence was neglected [the variation of $(n_z - n_x)$ is 5.10^{-4} between 20 °C and T_c].[26]

C. Derivation of the elastic-stiffness tensor

The elastic-stiffness tensor has the following form[30] in the monoclinic phase

$$\begin{pmatrix} c_{11} & c_{12} & c_{13} & 0 & c_{15} & 0 \\ c_{12} & c_{22} & c_{23} & 0 & c_{25} & 0 \\ c_{13} & c_{23} & c_{33} & 0 & c_{35} & 0 \\ 0 & 0 & 0 & c_{44} & 0 & c_{46} \\ c_{15} & c_{25} & c_{35} & 0 & c_{55} & 0 \\ 0 & 0 & 0 & c_{46} & 0 & c_{66} \end{pmatrix} \tag{3}$$

when it is referring to the three crystallographical axes of the orthorhombic phase (Voigt notation).

The coefficients c_{15}, c_{25}, c_{35}, and c_{46} have the same symmetry as the B_{2g} representation of the prototype point group (mmm). Thus, they change sign from one domain to another and vanish in the orthorhombic phase. The other coefficients belong to the A_g symmetry and keep the same value in both types of domains. They constitute the elastic-stiffness tensor in the orthorhombic phase.

The sound velocities v of the three acoustic waves propagating in the direction $\vec{Q}$ are determined by the following eigenvalues equation[35]:

$$\det\left(\sum_{j,k=1}^{3} c_{ijkl} q_j q_k - \rho v^2 \delta_{il}\right) = 0 \quad , \tag{4}$$

where q_j, q_k are the direction cosines of $\vec{Q}$, ρ is the density of the crystal, and c_{ijkl} is the full tensor notation of the elastic constants. The values of ρv^2, explicitly or implicitly defined, are given in Table I for all the modes propagating along the [100], [101], and similar directions. These modes were labeled with the γ_i notation already used by Vacher and Boyer.[35] However, these authors did not study the monoclinic system for which we had to distinguish [101] and [10$\bar{1}$] directions of the shear plane which are not equivalent in the monoclinic phase. Modes related to [10$\bar{1}$] have been labeled γ'_{16}, γ'_{17}, and γ'_{18}.

The derivation of the entire set of elastic constants from the sound velocities in a monoclinic material is not straightforward. They had to be determined at each temperature on a computer making use of the equations of Table I. The Brillouin lines related to the γ_5, γ_9, γ_{17}, γ'_{17} modes in both phases (and to the γ_{12} mode in the orthorhombic phase) were too weak to be detected, while γ_{11} and γ_{14} were only measured at room temperature. Thus, the experimental data provided us with ten different combinations of elastic constants (i.e., γ_1, γ_2, γ_3, γ_4, γ_7, γ_{10}, γ_{13}, γ_{15}, γ_{16}, γ_{18}) in the orthorhombic phase and 15 ones (the ten preceding ones, plus γ_6, γ_8, γ_{12}, γ'_{16}, γ'_{18}) in the monoclinic phase to determine all the components of the elastic-stiffness tensor (9 and 13 components, respectively) thus allowing some checking. The density was taken as[8] $\rho = 3.28 \times 10^3$ kg/m^3. As shown by our dilatometric measurements its temperature dependence could be neglected considering the accuracy of the other data.

In the orthorhombic phase, the c_{ii} components ($i = 1$ to 6) are explicit functions of γ_1, γ_2, γ_3, γ_4, γ_7, and γ_{18}. By contrast, γ_{10}, γ_{13}, and γ_{16} lead to pairs of values for the c_{12}, c_{23}, and c_{13} components through double-valued equations. We could discard the wrong determination of these constants by making use of the method suggested by Vacher and Boyer,[35] the incorrect determination leading to a pure transverse mode harder than a pure longitudinal one propagating in the same direction. A confirmation of the selected value of c_{13} was its weak dependence on temperature while the discarded value showed a strong dependence inconsistent with the other features of the investigated transition.

In the monoclinic phase, c_{22} and c_{66} are explicit functions of γ_4 and γ_2. The three quantities γ_6, γ_{18}, and γ'_{18} depend on c_{66} and on the additional constants c_{44} and c_{46} for which they supply consistent values. The expressions for γ_1, γ_3, γ_7, γ_8, γ_{16}, γ'_{16} constitute a system of six equations with $c_{11}, c_{33}, c_{55}, c_{13}, c_{15}, c_{35}$ as six unknown quantities. This system has two sets of solutions but only one is consistent with the results for the orthorhombic phase. Finally γ_{10} and γ_{12} (or γ_{13} and γ_{15}) lead to two second-degree equations with c_{12} and c_{25} (or c_{23} and c_{25}) as unknown quantities. There are two sets of solutions for the latter overdetermined system of four equations. Both are equally consistent with the additional room-temperature data for γ_{11} and γ_{14} (not used in the resolution). The two determinations of c_{12} and c_{23}

TABLE I. Expression of ρv^2 as a function of the elastic constants for the investigated Brillouin-scattering configurations, in the orthorhombic and monoclinic phases. In the first three columns are indicated the direction of propagation, the polarization (L for longitudinal or quasilongitudinal modes, T for transverse or quasitransverse modes), and the labeling (following the notation of Ref. 35) of the acoustic modes. The velocities of modes propagating along the [110] and [011] directions are not explicitly given in the monoclinic phase since ρv^2 are the roots of third-order equations.

Acoustic modes			Orthorhombic phase	Monoclinic phase
[100]	L	γ_1	c_{11}	$\frac{1}{2}\{c_{11}+c_{55}+[(c_{11}-c_{55})^2+4c_{15}^2]^{1/2}\}$
	T	γ_2	c_{66}	c_{66}
	T	γ_3	c_{55}	$\frac{1}{2}\{c_{11}+c_{55}-[(c_{11}-c_{55})^2+4c_{15}^2]^{1/2}\}$
[010]	L	γ_4	c_{22}	c_{22}
	T	γ_5	c_{44}	$\frac{1}{2}\{c_{44}+c_{66}+[(c_{44}-c_{66})^2+4c_{46}^2]^{1/2}\}$
	T	γ_6	c_{66}	$\frac{1}{2}\{c_{44}+c_{66}-[(c_{44}+c_{66})^2+4c_{46}^2]^{1/2}\}$
[001]	L	γ_7	c_{33}	$\frac{1}{2}\{c_{33}+c_{55}+[(c_{33}-c_{55})^2+4c_{35}^2]^{1/2}\}$
	T	γ_8	c_{55}	$\frac{1}{2}\{c_{33}+c_{55}-[(c_{33}-c_{55})^2+4c_{35}^2]^{1/2}\}$
	T	γ_9	c_{44}	c_{44}
[110]	L	γ_{10}	$\frac{1}{4}\{c_{11}+c_{22}+2c_{66}+[(c_{11}-c_{22})^2+4(c_{12}+c_{66})^2]^{1/2}\}$	$\gamma^3-A\gamma^2+B\gamma-C=0$ with $A=\frac{1}{2}(c_{11}+c_{22}+c_{44}+c_{55}+2c_{66})$ $B=\frac{1}{4}[(c_{11}+c_{66})(c_{22}+c_{66})+(c_{11}+c_{66})(c_{44}+c_{55})+(c_{22}+c_{66})(c_{44}+c_{55})-(c_{12}+c_{66})^2-c_{15}^2-c_{25}^2]$ $C=\frac{1}{8}[(c_{11}+c_{66})(c_{22}+c_{66})(c_{44}+c_{55})-(c_{44}+c_{55})(c_{12}+c_{66})^2+2c_{15}c_{25}(c_{12}+c_{66})-c_{15}^2(c_{22}+c_{66})-c_{25}^2(c_{11}+c_{66})]$
	T	γ_{11}	$\frac{1}{4}\{c_{11}+c_{22}+2c_{66}-[(c_{11}-c_{22})^2+4(c_{12}+c_{66})^2]^{1/2}\}$	
	T	γ_{12}	$\frac{1}{2}(c_{44}+c_{55})$	
[011]	L	γ_{13}	$\frac{1}{4}\{c_{22}+c_{33}+2c_{44}+[(c_{33}-c_{22})^2+4(c_{23}+c_{44})^2]^{1/2}\}$	$\gamma^3-A'\gamma^2+B'\gamma-C'=0$ with $A'=\frac{1}{2}(c_{33}+c_{22}+c_{66}+c_{55}+2c_{44})$ $B'=\frac{1}{4}[(c_{33}+c_{44})(c_{22}+c_{44})+(c_{33}+c_{44})(c_{66}+c_{55})\times(c_{22}+c_{44})(c_{66}+c_{55})-(c_{23}+c_{44})^2-c_{25}^2-c_{35}^2]$ $C'=\frac{1}{8}[(c_{33}+c_{44})(c_{22}+c_{44})(c_{55}+c_{66})-(c_{55}+c_{66})(c_{23}+c_{44})^2+2c_{25}c_{35}(c_{23}+c_{44})-c_{35}^2(c_{22}+c_{44})-c_{25}^2(c_{33}+c_{44})]$
	T	γ_{14}	$\frac{1}{4}\{c_{22}+c_{33}+2c_{44}-[(c_{33}-c_{22})^2+4(c_{23}+c_{44})^2]^{1/2}\}$	
	T	γ_{15}	$\frac{1}{2}(c_{55}+c_{66})$	
[101]	L	γ_{16}	$\frac{1}{4}\{c_{11}+c_{33}+2c_{55}+[(c_{33}-c_{11})^2+4(c_{13}+c_{55})^2]^{1/2}\}$	$\frac{1}{4}\{c_{11}+c_{33}+2c_{55}+2c_{15}+c_{35}+[(c_{11}-c_{33}+2c_{15}-2c_{35})^2+4(c_{15}+c_{13}+c_{35}+c_{55})^2]^{1/2}\}$
	T	γ_{17}	$\frac{1}{4}\{c_{11}+c_{33}+2c_{55}-[(c_{33}-c_{11})^2+4(c_{13}+c_{55})^2]^{1/2}\}$	$\frac{1}{4}\{c_{11}+c_{33}+2c_{55}+2c_{15}+c_{35}-[(c_{11}-c_{33}+2c_{15}-2c_{35})^2+4(c_{15}+c_{13}+c_{35}+c_{55})^2]^{1/2}\}$
	T	γ_{18}	$\frac{1}{2}(c_{44}+c_{66})$	$\frac{1}{2}(c_{44}+c_{66}+2c_{46})$
[10$\bar{1}$]	L	γ'_{16}	Same as γ_{16}	$\frac{1}{4}\{c_{11}+c_{33}+2c_{55}-2c_{15}-2c_{35}+[(c_{11}-c_{33}-2c_{15}+2c_{35})^2+4(-c_{15}+c_{13}-c_{35}+c_{55})^2]^{1/2}\}$
	T	γ'_{17}	Same as γ_{17}	$\frac{1}{4}\{c_{11}+c_{33}+2c_{55}-2c_{15}-2c_{35}-[(c_{11}-c_{33}-2c_{15}+2c_{35})^2+4(-c_{15}+c_{13}-c_{35}+c_{55})^2]^{1/2}\}$
	T	γ'_{18}	Same as γ_{18}	$\frac{1}{2}(c_{44}+c_{66}-2c_{46})$

were very close to each other while the relative difference between the two possible values of c_{25} was approximately 20%. Both values of c_{25} will be given in the following discussion of the results.

III. EXPERIMENTAL RESULTS

A. Thermal-strain tensor

The temperature dependence of the spontaneous monoclinic shear is plotted in Fig. 2.- On heating, e_5 decreases from $(789 \pm 2) \times 10^{-5}$ rad (27'8" ±4") at 22 °C and vanishes at $T_c = 124.40$ °C (however, this temperature was taken with an uncalibrated probe and the absolute value of T_c is known to ±1 °C). With the polished parallelepiped-shaped crystals, we saw first a slight rounding instead of a clear cancellation at T_c. But this effect was clearly due to internal stresses in the sample since it disappeared after annealing at 350 °C for 24 h. It was not observed in the as-grown crystal.

We could not observe any broadening of peaks since their width was always equal to the instrumental width (30"), except within 0.02 °C of the transition where no measurement was possible because of the peaks overlap and of the sample temperature instability. However, for $T = (T_c - 0.024\,°C)$ we could measure a shear as small as 28" and for $T > (T_c + 0.05\,°C)$ we could observe only one peak of 30"

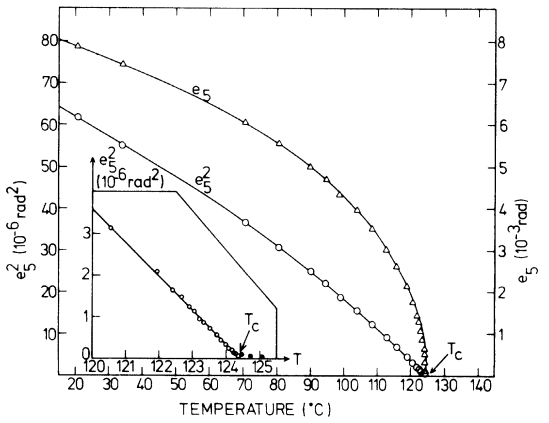

FIG. 2. Temperature dependence of the spontaneous monoclinic shear e_5 and of its square. Circles and triangles: experimental values deduced from γ-ray-diffractometry measurements. Solid lines: theoretical fit obtained from the phenomenological model including a sixth-order term in the free-energy expansion Eq. (8) (see Sec. IV). Measurements performed on the internally stressed sample before annealing are distinguished by filled dots in the lower inset. The transition is detected at 124.40 °C.

width, showing that within this accuracy the cancellation of e_5 is continuous. Moreover, no thermal hysteresis was observed on cooling; if any exists, it is smaller than 0.02 °C. By contrast, the thermal hysteresis of the first-order transition of KH_2PO_4 (KDP) measured[36] on the same diffractometer was 0.07 °C.

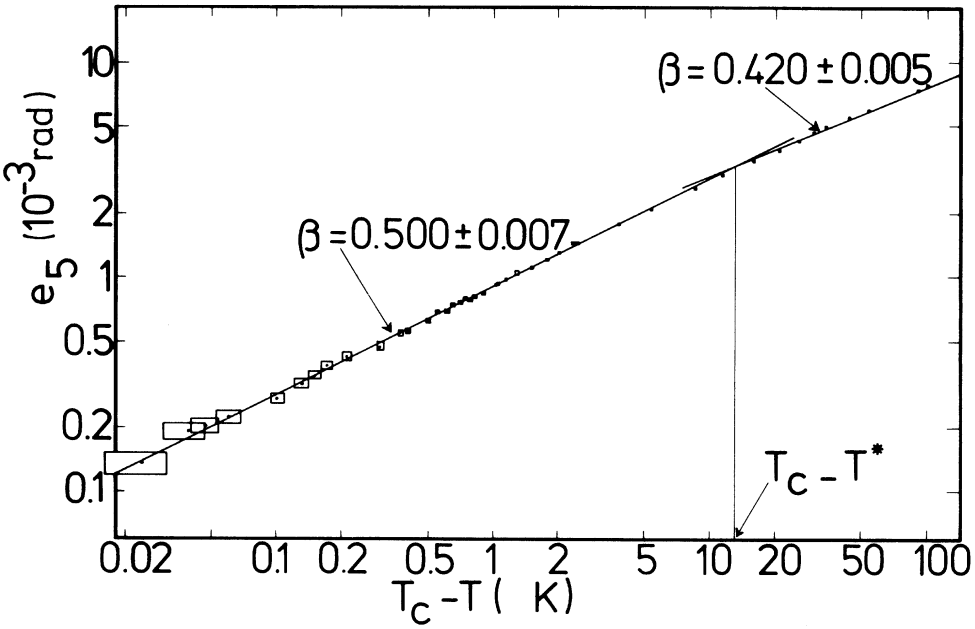

FIG. 3. Logarithmic plot of the temperature dependence of e_5. Experimental uncertainties are represented by empty rectangles for $T_c - T \leq 1$ °C. The two straight lines correspond to formulas (5) and (6). They give accurate values of the critical exponents. $\beta = 0.500 \pm 0.007$ for $T_c \geq T \geq T^*$ and $\beta = 0.420 \pm 0.005$ for $T \leq T^*$. The "crossover" temperature T^* corresponds to $T_c - T^* = 13$ °C.

The square of e_5 is also plotted on Fig. 2. We can see that it varies linearly in an interval of 13 °C below T_c. From this plot we deduce that e_5 vanishes with a critical exponent $\beta = 0.5$. A more accurate value of β can be deduced using the logarithmic plot of Fig. 3. We find that

$$e_5 = A\,(T_c - T)^{\beta} \ , \tag{5}$$

with $T_c = 124.40 \pm 0.02$ °C and that

$$\begin{aligned} &A = 0.910 \times 10^{-3}, \quad \beta = 0.500 \pm 0.007 \ , \\ &\text{for } T_c \geq T \geq (T_c - 13\,^{\circ}\text{C}) \ ; \\ &A = 1.130 \times 10^{-3}, \quad \beta = 0.420 \pm 0.005 \ , \\ &\text{for } (T_c - 13\,^{\circ}\text{C}) \geq T \geq 25\,^{\circ}\text{C} \ . \end{aligned} \tag{6}$$

These results are in good agreement with the previous works of Budin *et al.*[9] and Fousek *et al.*[26] Budin *et al.*[9] have measured e_5 on a $La_{0.25}Nd_{0.75}P_5O_{14}$ sample by an optical method. They found $\beta = 0.417$ for the whole temperature range ($20 \leq T \leq T_c - 0.5$ °C) but their measurements were performed on a stressed crystal with an accuracy of $\pm 20''$ while ours are made on a free sample with an accuracy of $\pm 4''$. Fousek *et al.*[26] have found the same two critical exponents for the spontaneous birefringence (measured on a thin plate of LaP_5O_{14} between crossed polarizers) but with a different temperature of "crossover" ($T_c - T^* = 3.5$ instead of 13 °C).

Typical recording of our dilatometric measurements along the crystallographic axes are reproduced on Fig. 4. Thermal strains are continuous at the transition detected at $T_c = 125 \pm 1$ °C for LaP_5O_{14} samples and $T_c = 143$ °C for NdP_5O_{14} ones. In both materials, they have a linear temperature dependence on both sides of T_c ($-13 \leq T - T_c \leq 80$ °C) with larger expansion coefficients in the monoclinic phase. These coefficients decrease between $T_c - 13$ and $T_c - 40$ °C and remain constant below $T_c - 40$ °C. Their values are reproduced in Table II at room temperature and on both sides of T_c.

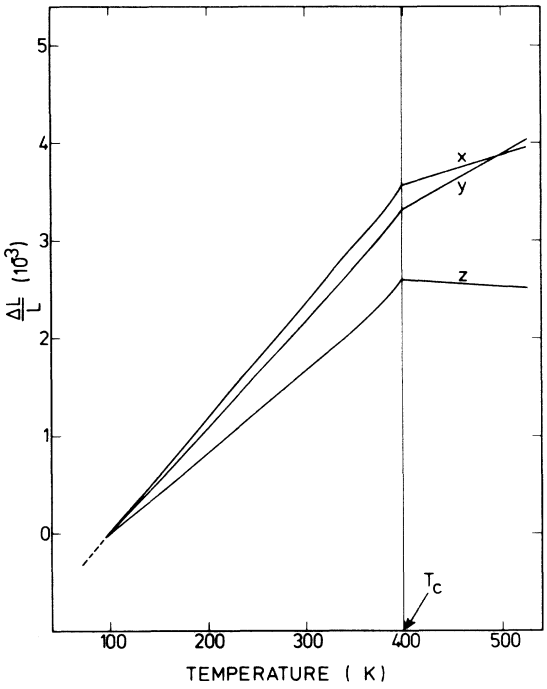

FIG. 4. Thermal expansion of LaP_5O_{14} along the three crystallographic axes. The transition is detected at $T_c = 125 \pm 1$ °C.

TABLE II. Expansion coefficients of LaP_5O_{14} and NdP_5O_{14}. In the next to last column, we indicate the difference between the expansion coefficients on both sides of T_c. These differences are nearly identical in LaP_5O_{14} and NdP_5O_{14}. They can also be derived from the phenomenological model. The results are given in the last column. Note the small value of α_z above T_c in the two compounds.

Expansion coefficient (10^6)		20 °C	$T_c - 1$ °C	$T > T_c$	Jump at T_c Experimental	Jump at T_c Theoretical
LaP_5O_{14}	α_x	11.8 ± 0.4	13.7 ± 0.4	2.9 ± 0.4	10.8 ± 0.8	11.23
	α_y	10.9 ± 0.4	12.7 ± 0.4	6.4 ± 0.4	6.3 ± 0.8	6.70
	α_z	8.3 ± 0.4	11 ± 0.6	−0.5 ± 0.3	11.5 ± 0.9	12.55
NdP_5O_{14}	α_x	11.5 ± 0.7	14.6 ± 0.7	3.7 ± 0.5	10.9 ± 1.2	11.23
	α_y	11.2 ± 0.7	15.4 ± 0.7	8.8 ± 0.5	6.60 ± 1.1	6.70
	α_z	6.5 ± 0.7	11.5 ± 1	+0.4 ± 0.3	11.1 ± 1.3	12.55

B. Sound velocities

The temperature dependence of ρv^2 for all the observed acoustic modes is plotted in Fig. 5. Accurate values of the velocities are listed in Table III for 20, 125, and 200 °C. However, as we already pointed out, the lines corresponding to γ_5, γ_9, γ_{17}, γ'_{17} in both phases and to γ_{12} in the orthorhombic phase were too weak to be detected even with a 1-W excitation, and γ_{11} and γ_{14} were only measured at room temperature. The velocities of all the other modes are continuous. All but γ_2 and γ_6 exhibit anomalies related to the transition which was measured at 126 °C in this experiment. (Here again, its absolute value is known with an uncertainty of ±1 °C.)

We found two transverse modes whose velocities nearly vanish at T_c in agreement with Aubry and Pick.[37] The decrease of the velocity of the first one, γ_3 (wave vector $\vec{Q} \parallel [100]$, polarization $\parallel [001]$), was followed down from 3300 m/s at 20 °C to 170 m/s at

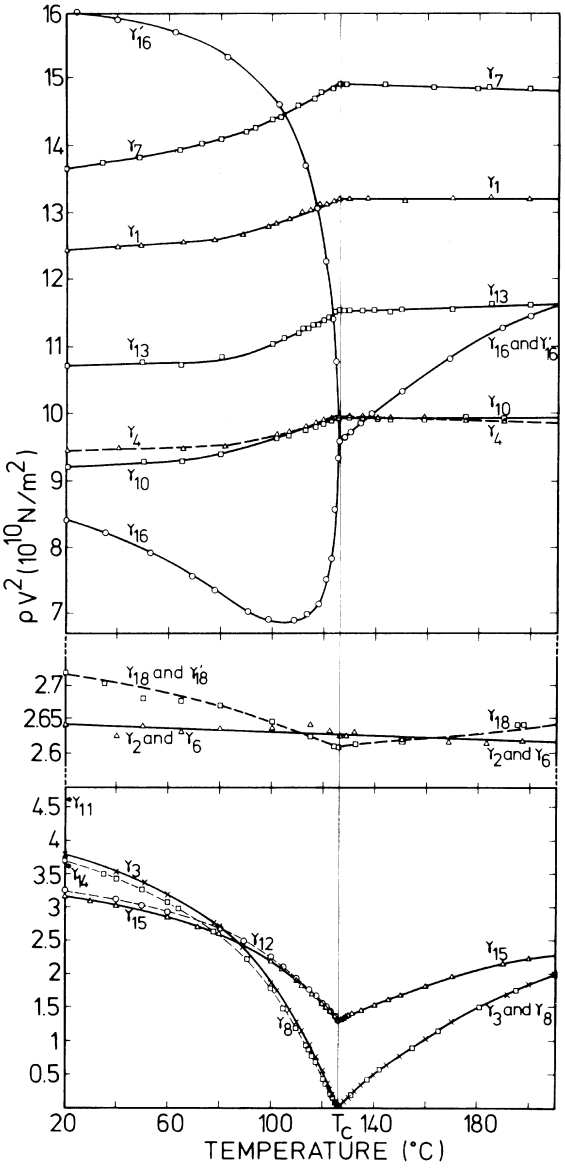

FIG. 5. Temperature dependence of ρv^2 in the [100], [110], and similar directions, between 20 and 200 °C, deduced from Brillouin-scattering measurements. The upper part of the figure is relative to the longitudinal modes, the central and the lower part to the transverse-acoustic modes. The directions of propagation of the γ_i modes are given in Table I. Measurements of γ_{11} and γ_{14} modes represented by stars were only performed at room temperature, while we could not follow the γ_{12} mode in the orthorhombic phase because of its weak intensity.

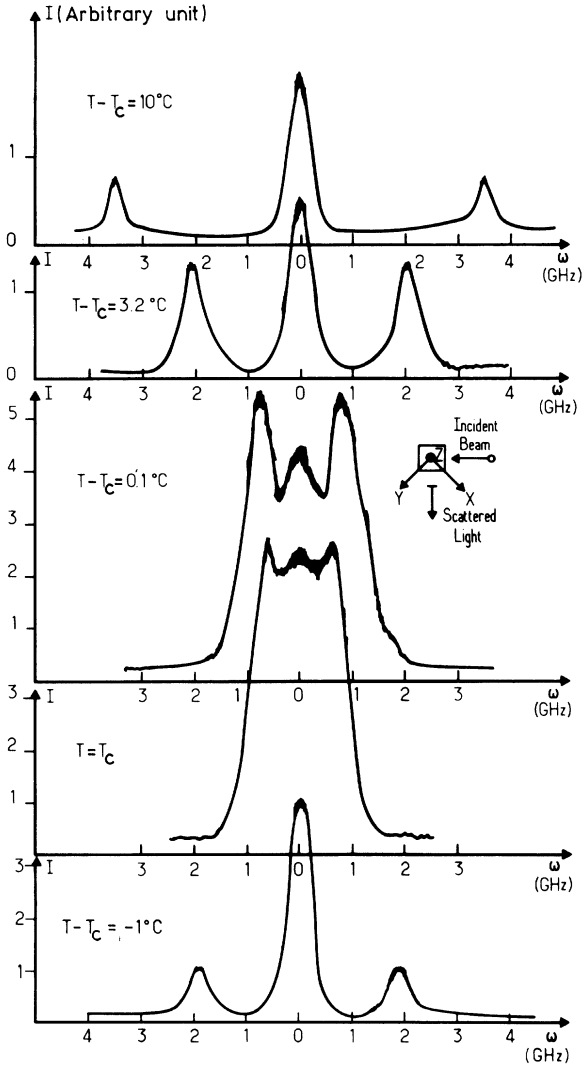

FIG. 6. Temperature dependence of the Brillouin spectra of the γ_3 mode in $(x+y)(z,x+y)(x-y)$ scattering geometry on both sides of T_c. The intensity of the Rayleigh line has been strongly reduced by making use of a polarizer to analyze the scattered light. No broadening of the Brillouin lines has been detected. The sound velocity of the transverse-acoustic mode is found to be nearly 170 m/s at T_c.

TABLE III. Sound velocities of LaP_5O_{14} at 20, 126, and 200 °C deduced from Brillouin measurements. The meaning of the γ_i notation is given in Table I and Ref. 35. The γ_5, γ_9, γ_{17}, and γ'_{17} modes were too weak to be detected. Besides, we could not detect any difference between γ_2 and γ_6 on one hand, and γ_{18} and γ'_{18} on the other hand. The experimental uncertainty is ±25 m/s.

Mode labeling	Monoclinic phase (20 °C) (10^3 m/s)	Orthorhombic phase (T_c = 126 °C) (10^3 m/s)	(200 °C) (10^3 m/s)
γ_1	6.16	6.35	6.35
γ_2 and γ_6	2.84	2.83	2.82
γ_3	3.40	0.17	2.37
γ_4	5.37	5.51	5.49
γ_7	6.45	6.75	6.72
γ_8	3.35	0.17	2.37
γ_{10}	5.30	5.50	5.50
γ_{11}	3.66	. . .	. . .
γ_{12}	3.15	2.00	. . .
γ_{13}	5.71	5.93	5.95
γ_{14}	3.34	. . .	. . .
γ_{15}	3.11	1.99	2.61
γ_{16}	5.07	5.40	5.91
γ'_{16}	6.99	5.40	5.91
γ_{18} and γ'_{18}	2.87	2.82	2.83

T_c. The second one, γ_8 ($\vec{Q} \parallel [001]$, polarization $\parallel$ [100]), has already been reported.[18] Its velocity is always a little smaller than the former one in the monoclinic phase. This has been carefully verified using the back reflection device to simultaneously observe the two soft modes. In the orthorhombic phase, both velocities are equal and increase. Figure 6 shows the evolution of the Brillouin spectra for the γ_8 mode near T_c. Here again, we could detect neither a thermal hysteresis (if any, it is smaller than 0.2 °C) nor a jump of ρv^2 at T_c ($< 2 \times 10^7$ N/m^2). Their observed width always remained equal to the instrumental width (600 MHz) except perhaps for $-0.4 \leq T - T_c \leq +1$ °C, where they were not well separated from the Rayleigh component. Thus, we could never determine the acoustic attenuation which is related to the intrinsic linewidth,[38] in contrast with other ferroelastic materials such as $Pb_3(PO_4)_2$,[39] $Gd_2(MoO_4)_3$,[40] and Hg_2Cl_2,[41] for which a critical increase of the width of the soft acoustic modes has been detected. The intensities of the γ_3 and γ_8 modes of LaP_5O_{14} increase slightly more rapidly than $1/v^2$ on approaching the transition temperature. We also observed an apparent increase of the intensity of the Rayleigh component. This and the incomplete vanishing of the two soft mode velocities can perhaps be related to an interaction of these modes with a central peak. However, the accuracy of our experiment did not permit us to clarify this point by resolving the Rayleigh component and the Brillouin ones in the close vicinity of the transition.

The γ_{18} and γ'_{18} mode velocities could not be distinguished, even when we simultaneously measured them with the back reflection device, as is shown in Fig. 7. Their common frequency is slowly temperature dependent with a slight minimum at T_c. Also, we did not detect any difference between the velocities of the γ_2 and γ_6 modes. They slowly decreased with the temperature and did not show any anomaly at T_c. Since the determination of the elastic constants is very sensitive to the difference between the velocities of the γ_2 and γ_{18} modes, we measured it as carefully as possible by alternatively looking at the light scattered by two crystals put together in the oven. We observed that the velocity for γ_2 is greater than for γ_{18} between 110 and 160 °C and smaller outside this temperature range.

The velocities of the γ_{16} and γ'_{16} modes are strongly temperature dependent. As shown in Fig. 7, we observed an important softening of γ'_{16} (40% of ρv^2 between 20 °C and T_c) and a minimum of γ_{16} near 105 °C. First the corresponding Brillouin lines separate between 20 and 80 °C, then they approach each other to merge at T_c. They coincide in the orthorhombic phase where the [101] and [10$\bar{1}$] propagation directions are equivalent. (In this phase,

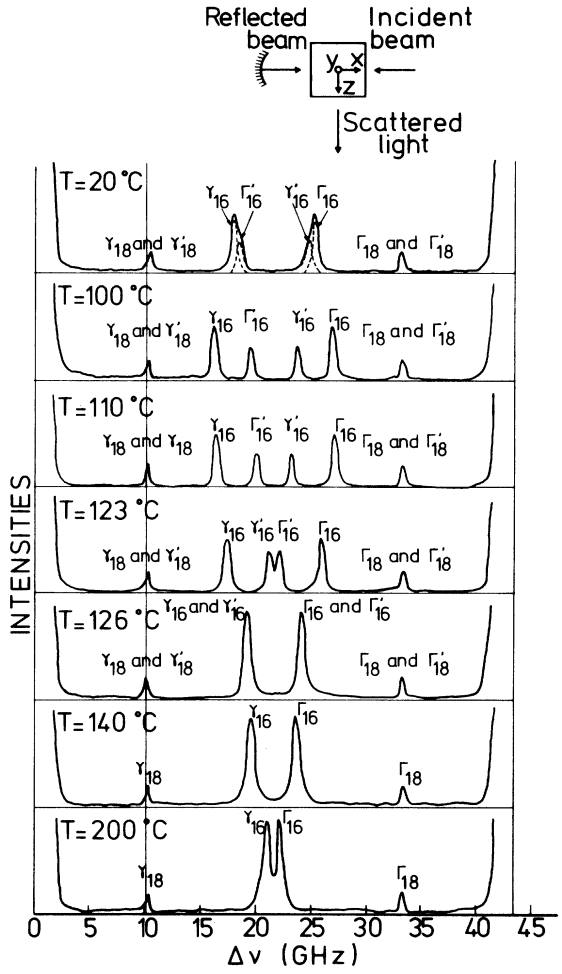

FIG. 7. Temperature dependence of the Brillouin spectra related to [101] (γ_{16} and γ_{18} lines) and [10$\bar{1}$] directions (γ'_{16} and γ'_{18} lines). The Γ notation corresponds to anti-Stokes scattering. Table I shows that these directions are not equivalent in the monoclinic phase. However, when they are simultaneously observed with a back-reflection-mirror device (Ref. 34), we cannot detect any difference between the velocities of the γ_{18} and γ'_{18} modes which exhibit a slight minimum at T_c. On the contrary, the velocities of the γ_{16} and γ'_{16} modes are clearly different below T_c. One can note their slight separation on heating from 20 to 80 °C corresponding to an increase of $|c_{15}|$ and $|c_{35}|$ in this temperature range.

the temperature variations of ρv^2 above T_c exactly reproduce those of the γ_3 and γ_8 modes.)

The intensities of all modes except those for γ_{12}, γ_3, γ_8 remained nearly constant in the whole temperature range and the width of all modes was always equal to the instrumental width.

As we shall now see, the sometimes intricate behavior of all the observed sound velocities can be explained by the temperature dependence of the elastic-stiffness tensor-components, involving either smooth variations or anomalies of a type usual for a phase transition.

C. Elastic-stiffness tensor

The temperature dependence of all the elastic constants is shown in Fig. 8. All are continuous. Their precise values at $T=20$, 125, and 200 °C are listed in Table IV. The c_{55} component, which is the inverse susceptibility related to e_5, vanishes at $T_c = 126 \pm 1$ °C with the critical exponent $\gamma = \gamma' = 1.0 \pm 0.02$ and thus increases linearly for $-13 \leq T - T_c \leq 18$ °C on both sides of T_c with a slope ratio of 2.90 ± 0.06. In the orthorhombic phase this stiffness component is directly proportional to the squared frequency of the γ_3 and the γ_8 modes while its value is larger in the monoclinic phase.

The c_{66} component, like γ_2, slowly decreases on heating without any anomaly at the transition while c_{44} exhibits a weak minimum at T_c. $|c_{46}|$ is always smaller than 10^8 N/m^2 in the monoclinic phase since it is related to the differences between γ_{18} and γ'_{18} and between γ_2 and γ_6 which were not detected.

The c_{ij} components (with i and $j \leq 3$) have a linear temperature dependence with different slopes on either sides of T_c. c_{11}, c_{22}, and c_{33} coincide, respectively, with γ_1, γ_4, and γ_7 in the orthorhombic phase and are smaller below T_c.

Finally, the behavior of c_{15}, c_{35}, and of the two possible determinations of c_{25} resemble each other. On cooling from T_c, first their absolute values rapidly increase to maxima in the 60–80 °C range and then slowly decrease. This decrease is not a stray effect coming from uncertainties in the resolution of the γ_i system. Actually, an expansion near T_c of γ_{16} and γ'_{16} leads to

$$\gamma_{16} - \gamma'_{16} = 4(c_{15} + c_{35}) \ ; \tag{7}$$

thus the decrease of $|c_{15} + c_{35}|$ below 80 °C is directly related to the observed decreasing distance between γ_{16} and γ'_{16}. Note that these components which are equal to zero in the orthorhombic phase assume large values (of a similar magnitude as c_{66} which is not affected by the transition) very rapidly in the ferroelastic phase. It is striking that the crystal which is pseudo-orthorhombic from a crystallographic point of view has a pronounced monoclinic character with respect to the stiffness properties.

Let us now examine how the behavior of the elastic constants and of the thermal-strain tensor can be explained from a phenomenological point of view, using a Landau free-energy expansion having a small number of coupling coefficients.

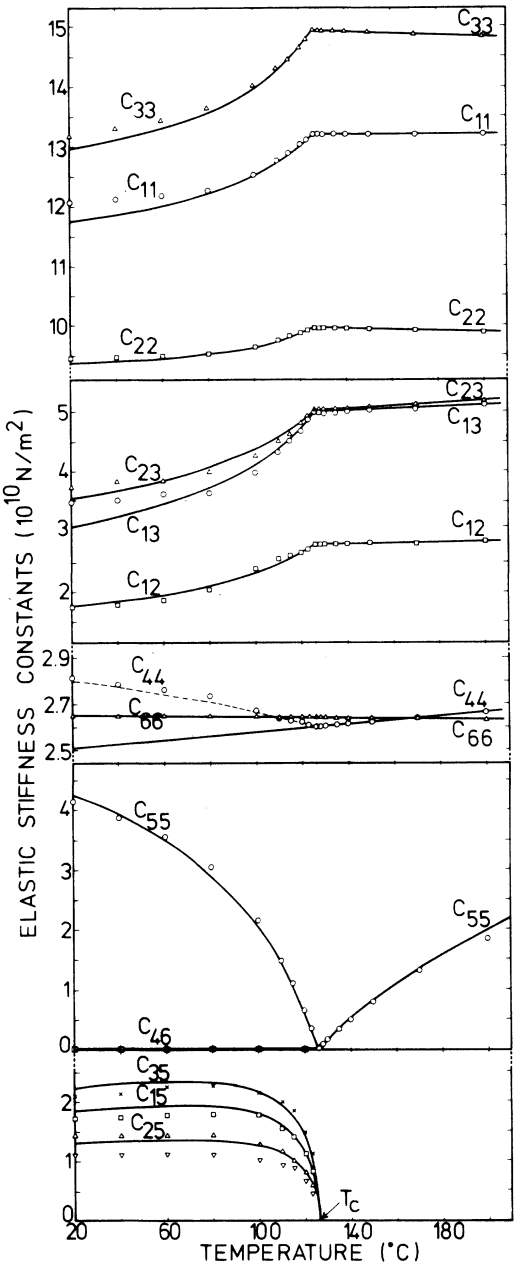

FIG. 8. Temperature dependence of the elastic-stiffness-tensor components. Triangles, circles, squares, and crosses: values deduced from the experiments by solving the system Eq. (4) for 17 values of T in both phases. c_{15},c_{25},c_{35} take opposite values in the two types of domains (only positive values are plotted). As explained at the end of Sec. II, we found two determinations of $|c_{25}|$ represented by triangles in the lower part of the figure. Solid lines: theoretical fit deduced from the phenomenological model limited to the fourth order. Dashed line: fit of c_{44} when an additional bilinear-coupling term between e_4 and the B_{3g} soft mode is taken into account.

IV. PHENOMENOLOGICAL THEORY

The set of our experimental results confirms that LaP_5O_{14} belongs to the simplest ferroelastic class studied by Cowley and Schwabl for which renormalization-group calculations[7] support the occurrence of classical behavior. Actually the investigated transition appears as a continuous one in the plots of all the measured quantities. Previous works had already shown this result but our γ-ray-diffractometry measurements, performed at an interval of 0.02 °C near the transition provide a more accurate basis to this assignment (Figs. 2 and 3). This continuity is seen as well in the absence of a thermal hysteresis in the elasticity and thermal expansion experiments. As noticed formerly by Toledano *et al.*,[18] the order parameter of the transition has the same symmetry B_{2g} as the monoclinic shear e_5; thus the transition is a proper ferroelastic one.[2] No effect of fluctuations is observed at the transition. Actually we did not find any broadening of the γ diffraction peaks or of the Brillouin lines and we found critical exponents of the classical type for e_5 ($\beta = 0.500 \pm 0.007$) and for the c_{55} elastic constant ($\gamma = 1.00 \pm 0.02$). Finally we checked that acoustic-mode velocities vanish at the transition for two propagation directions only (namely, [100] and [001]) and not in a whole plane in reciprocal space.[7] We can therefore expect to describe quantitatively the mechanical and elastic properties of LaP_5O_{14} with the help of the phenomenological Landau theory of phase transitions based on a B_{2g} order-parameter symmetry, even in the vicinity of the transition.

However, the spontaneous strain e_5 is not the only quantity possessing the B_{2g} symmetry and whose consideration is relevant to the transition. As Raman measurements have shown it, there are two temperature-dependent optical modes[21,22] whose squared frequencies have minima at T_c and which vary linearly on either side of T_c. The harder one has the B_{3g} symmetry and can be discarded, but the softer one is a B_{2g} mode and its associated normal coordinate Q should also be considered as a possible order parameter for the transition. Actually e_5 and Q, having the same symmetry, are bilinearly coupled, and strictly speaking the order parameter of the transition is a linear combination of e_5 and Q. However, as long as the frequency of the "bare" optic mode Q is considerably larger than that of the "bare" acoustic mode e_5, it can be shown[42] that the renormalized modes will remain almost purely optic and purely acoustic with a very little amount of mixing (2% in our case).

Besides, the coupling leaves the frequency of the optic mode ω_Q, almost unchanged, while the acoustic-mode frequency is significantly lowered (and vanishes at T_c). Consequently, the choice of e_5 as the "primary" order parameter would not account for

TABLE IV. Elastic constants of LaP_5O_{14} at 20, 126, and 200 °C. c_{15}, c_{25}, c_{35}, and c_{46} vanish above T_c because of the symmetry properties of the orthorhombic phase. According to the phenomenological model, they are positive in the domains with $e_5 > 0$ ($\beta < 90°$) and negative in the other type of domains. Two determinations of c_{25} are indicated (see text).

Elastic constant	Monoclinic phase (20 °C) (10^{10} N/m^2)	Orthorhombic phase ($T_c = 126$ °C) (10^{10} N/m^2)	(200 °C) (10^{10} N/m^2)
c_{11}	12.08 ± 0.20	13.21 ± 0.12	13.21 ± 0.12
c_{22}	9.46 ± 0.12	9.96 ± 0.12	9.89 ± 0.12
c_{33}	13.19 ± 0.20	14.94 ± 0.12	14.83 ± 0.12
c_{44}	2.80 ± 0.07	2.59 ± 0.07	2.65 ± 0.07
c_{55}	4.14 ± 0.10	0.010 ± 0.003	1.83 ± 0.05
c_{66}	2.64 ± 0.05	2.63 ± 0.05	2.62 ± 0.05
c_{12}	1.74 ± 0.30	2.79 ± 0.25	2.85 ± 0.25
c_{13}	3.53 ± 0.30	5.01 ± 0.25	5.13 ± 0.25
c_{23}	3.75 ± 0.30	5.03 ± 0.25	5.18 ± 0.25
c_{15}	± 1.71 ± 0.15	...	...
c_{25}	± 1.43 ± 0.20	...	...
	± 1.10 ± 0.20	...	...
c_{35}	± 2.09 ± 0.15	...	...
$\lvert c_{46}\rvert$	< 0.015	...	...

the strong temperature dependence which is observed for ω_Q in the Raman spectra.[21,22] By contrast, the choice of Q as the primary order parameter is likely to explain the simultaneous softening of an optic and an acoustic mode as already noticed by Scott.[25] Moreover, it will be shown below that this assumption provides us with a quantitative explanation of the experimental data.

We can note that the choice of either e_5 or Q as the primary order parameter for the transition is not a purely formal one but has a physical meaning since it indicates which one of the mechanical or the optical instabilities induces the transition and triggers the other one. The choice of Q has the meaning that the studied phase transition would still occur in a rigid lattice (a clamped crystal).

Thus, the Landau free-energy for this transition can be written as

$$F = F_Q + F_e + F_c \ ,$$

with

$$F_Q = (\tfrac{1}{2}\alpha) Q^2 + (\tfrac{1}{4}\beta) Q^4 \ ,$$

$$F_e = \tfrac{1}{2} \sum_{i,j=1,3} c_{ij}^0 e_i e_j + \tfrac{1}{2} \sum_{k=4,6} c_{kk}^0 e_k^2 \ , \qquad (8)$$

and

$$F_c = \gamma e_5 Q + \sum_{i=1,3} \delta_i e_i Q^2 \ .$$

F_Q contains the terms relative to the bare normal coordinate Q associated to the soft optic mode with B_{2g} symmetry. In agreement with the primary character of Q, we assume that $\alpha = a(T - T_0)$. F_e is the elastic energy of the crystal in the form adapted to the orthorhombic phase. F_c contains the coupling terms between Q and the components of the thermal-strain tensor.

To account for a second-order transition we assume that a and $\beta > 0$ and that the coefficients $a, \beta, c_{ij}^0, c_{kk}^0, \gamma, \delta_i$ are slowly temperature dependent. For the sake of simplification, we did not take into account the thermal expansion of the prototype phase which would lead to the introduction of linear terms in F. These are unimportant if one restricts the comparison of the theoretical predictions to the modification of thermal expansion observed at the transition. Also, we only kept the lowest-order coupling term between Q and the thermal-strain tensor, and neglected some of the coupling terms of fourth order. Their effect will be briefly discussed as well as that of higher-order terms.

With these assumptions, we can derive from the free-energy expansion the temperature dependence of the various quantities of interest. The equilibrium values of Q and e_i, in a mechanically free crystal, are determined by the cancellation of the first derivatives of F. The frequency of the soft optic mode and elastic-stiffness-tensor components are related to the second derivatives.[42] The resulting expressions are listed in Table V.

TABLE V. Calculated temperature dependence of the thermal-strain and elastic-stiffness-tensor components, and of Q and ω_Q, deduced from the free-energy expansion Eq. (8) in the paraelastic and ferroelastic phase. The transition occurs at $T_c = T_0 + \gamma^2/ac_{55}^0$. The i and j indices vary from 1 to 3. (s_{ij}^0) is the inverse matrix of (c_{ij}^0). We put: $t = (T - T_c)$, $t' = (T_c - T)$, $\beta' = \beta - 2\sum_{i,j=1,3} s_{ij}^0 \delta_i \delta_j$, $g = ac_{55}^0/\gamma^2 = 1/(T_c - T_0)$, and $g' = 2(\beta/\beta')g$. The $\pm$ signs correspond to the two types of domains.

	Orthorhombic phase	Monoclinic phase
Q	0	$\pm (at'/\beta')^{1/2}$
e_5	0	$\mp \frac{\gamma}{c_{55}^0}(at'/\beta')^{1/2}$
e_i	0	$-\left(\sum_{j=i}^{3} s_{ij}^0 \delta_j\right)(at'/\beta')$
e_4	0	0
e_6	0	0
$m\omega_Q^2$	$a\left(t + \frac{1}{g}\right)$	$a\left(\frac{2\beta}{\beta'}t' + \frac{1}{g}\right)$
c_{55}	$c_{55}^0 \frac{gt}{1+gt}$	$c_{55}^0 \frac{g't'}{1+g't'}$
c_{i5}	0	$\mp \delta_i \left(\frac{2c_{55}^0}{\beta}\right)^{1/2} \left(\frac{g't'}{1+g't'}\right)^{1/2}$
c_{ij}	c_{ij}^0	$c_{ij}^0 - \frac{2\delta_i\delta_j}{\beta}\frac{g't'}{1+g't'}$
c_{44}	c_{44}^0	c_{44}^0
c_{66}	c_{66}^0	c_{66}^0
c_{46}	0	0

As shown by this table, all the quantities are expected to be continuous at the transition which occurs at $T_c = T_0 + (\gamma^2/ac_{55}^0)$. As previously noted[42,43] the coupling between Q and e_5 produces an upward shift of the transition temperature in a mechanically free crystal, T_0 being the temperature where ω_Q would vanish in the absence of coupling. The spontaneous quantities e_5 and Q vary as $\sim (T_c - T)^{1/2}$ while the $e_i (i = 1 \text{ to } 3)$ depend linearly on temperature because of the quadratic coupling with Q.

This coupling has another interesting effect: While both c_{55} and ω_Q^2 are predicted to increase linearly on either side of T_c (at least in a temperature interval such as gt, or $g't' \ll 1$), the ratio of the slopes below and above the transition is $(2\beta/\beta')$ instead of 2 as would be the case in the absence of coupling. Outside the preceding temperature interval, c_{55} increases more slowly and reaches a saturation value equal to c_{55}^0. We can note that this saturation is predicted without need of introducing terms of order higher than 4 in the free energy: It results from the coupling between e_5 and Q. Besides c_{55} and ω_Q are related in both phases by the Miller and Axe formula[24]

$$c_{55} = c_{55}^0 - \gamma^2/m\omega_Q^2 \tag{9}$$

(where m is the mass of the soft optic mode), which explains the simultaneous softening of the acoustic modes related to c_{55} and of the optic mode. When this mode softens in the prototype phase, ω_Q^2 strongly decreases and because of the coupling between e_5 and Q, c_{55} vanishes before ω_Q^2, inducing the ferroelastic transition.

In the framework of the present phenomenological theory, the temperature dependence of the 13 elastic constants depends on only four "reduced" parameters of the expansion, namely $(\delta_i/\beta^{1/2})$ $(i = 1, 2, \text{ and } 3)$ and (γ^2/a), in addition to the c_{ij}^0 parameters. These variations are therefore related to each other. In particular, the spontaneous quantities c_{i5}/δ_i and $\Delta c_{ij}/\delta_i\delta_j$ with $i,j = 1$ to 3, where Δc_{ij} is the difference between c_{ij} values in the monoclinic phase and in the orthorhombic phase extrapolated below T_c, are independent of i and j.

These results are clearly in good qualitative agreement with the experimental observations. Before discussing in more detail their comparison with the experimental data, let us examine the quantitative fitting to these data which leads to a numerical determination of the relative values of the various parameters of the expansion.

First we identify the c_{ij}^0, $(i,j = 1 \text{ to } 3)$ c_{44}^0, and c_{66}^0 coefficients with the slowly temperature-dependent elastic constant c_{ij}, c_{44}, and c_{66} in the orthorhombic phase or with their extrapolated values below T_c. c_{55}^0 and the four coupling coefficients mentioned above $(\delta_i/\sqrt{\beta}$ and $\gamma^2/a)$ are determined to simultaneously fit the temperature dependence of c_{55} in the whole temperature range and of c_{11}, c_{22}, and c_{33} near T_c. Finally, (β/a^2) is chosen to account for the linear temperature dependence of e_5^2 below the transition. Since only the product aQ^2 is determined, all the parameters of the free-energy expansion can be expressed as functions of the coefficient "a" of Q^2. Their values are given in Table VI.

On the basis of these values the predicted temperature dependence of the elastic constants is plotted on Fig. 8. These variations correspond to isothermal conditions. However, the magnitude of the difference between the isothermal and adiabatic values could be evaluated on the basis of the known specific

TABLE VI. Values of the coefficients of the free-energy expansion Eq. (8). All the c_{ij} coefficients are slowly temperature dependent and are given at T_c. (c^0_{55} is constant over the whole temperature range.)

Coefficient	Numerical value	Coefficient	Numerical value
$\frac{\beta}{a^2}$	4.48×10^{-3}	c^0_{33}	14.94×10^{10}
$\frac{\gamma}{\sqrt{a}}$	3.36×10^{6}	c^0_{44}	2.59×10^{10}
$\frac{\delta_1}{a}$	7.14×10^{3}	c^0_{55}	6.62×10^{10}
$\frac{\delta_2}{a}$	5.01×10^{3}	c^0_{66}	2.63×10^{10}
$\frac{\delta_3}{a}$	8.62×10^{3}	c^0_{12}	2.79×10^{10}
c^0_{11}	13.21×10^{10}	c^0_{13}	5.01×10^{10}
c^0_{22}	9.96×10^{10}	c^0_{23}	5.03×10^{10}

heat[27] and thermal expansion of the crystal and is found to affect negligibly the result $[(c^S_{11}-c^T_{11})/c^T_{11}\approx 2\times10^{-3};\ (c^S_{55}-c^T_{55})/c^T_{55}\lesssim 5\times10^{-3}]$. Therefore, the experimental data deduced from Brillouin scattering, which correspond to adiabatic conditions, can be directly compared to the calculated ones which are also given in Fig. 8.

The experimental behavior is satisfactorily reproduced for most components in the whole range of their measured variations. Consistently, the best agreement is obtained in the vicinity of the transition ($T_c-13\,^\circ\mathrm{C}\leq T\leq T_c$). We note that the larger of the two values determined of c_{25} is better accounted for by the model. Also, the calculated thermal expansion coefficients ($\Delta e_i/\Delta T$) coincide with the experimental values near T_c (see Table II) when we do not take into account the slowly temperature-dependent part of the thermal expansion which is not related to the occurrence of the ferroelastic transition. In addition, a large shift of the transition temperature, $(T_c-T_0)=170\,^\circ\mathrm{C}$, is predicted from the determined value of the coupling coefficient ($\gamma/\sqrt{a}$) which matches accurately the value ($161\pm11\,^\circ\mathrm{C}$) deduced from the Raman spectra.[21,22]

Below the former range of temperature, the various quantities are more slowly temperature dependent than the model predicts. This saturation effect is not unexpected and could be accounted for by the introduction of higher-order terms in the free-energy expansion. As an example, an additional $\frac{1}{6}\epsilon Q^6$ term in Eq. (8) leads to

$$e_5^2=\frac{\gamma^2}{c^{02}_{55}}\frac{\beta'}{2\epsilon}\left[\left(1+\frac{4a\,\epsilon(T_c-T)}{\beta'^2}\right)^{1/2}-1\right], \quad (10)$$

giving an excellent fit of the accurate γ-ray-diffractometry measurements if we take $\epsilon/a^3=4.52\times10^{-8}$ as seen in Fig. 2 (solid line). This result shows that the use of two critical exponents (see Sec. III A) is not necessary to describe the temperature dependence of e_5.

On the other hand, the experimental data obtained for the transition of the isostructural rare-earth pentaphosphates ($RePO_{14}$ with Re=La to Tb) coincide with the data of LaP_5O_{14} when we take into account the shift of the transition temperature. This is the case of the soft-optic-mode behavior in NdP_5O_{14} (Ref. 22) and TbP_5O_{14} (Ref. 23), the acoustic mode in $La_{0.5}Nd_{0.5}P_5O_{14}$ (Ref. 19), the optical shear measurements in $La_{0.25}Nd_{0.75}P_5O_{14}$ (Ref. 9), as well as our thermal-expansion data on NdP_5O_{14} (see Table II).

Likewise, the jump of specific heat derived from the free energy Eq. (8) is[5]

$$\Delta C=T_c\frac{a^2}{2\beta'}, \quad (11)$$

for which we find 4.7 $\mathrm{cal\,g^{-1}\,^\circ C^{-1}}$ for LaP_5O_{14} and 4.9 $\mathrm{cal\,g^{-1}\,^\circ C^{-1}}$ for both NdP_5O_{14} ($T_c=143\,^\circ\mathrm{C}$) and PrP_5O_{14} ($T_c=139\,^\circ\mathrm{C}$) in good agreement with the experimental value 5.3 ± 0.4 $\mathrm{cal\,g^{-1}\,^\circ C^{-1}}$ deduced from the work of Loiacono *et al.*[27] for the two latter materials.

Finally, the phenomenological model allows an evaluation of the pressure dependence of the soft optic mode. First, from Clapeyron's relation[5] we deduce the displacement of the transition temperature

$$(dT_c/dp)=2\sum_{i,j=1,3}s^0_{ij}(\delta_j/a)=18.9\,^\circ\mathrm{C/kbar}, \quad (12)$$

s^0_{ij} being the elastic compliance tensor for $T\geq T_c$.

The signs of the jumps of the expansion coefficients at T_c leads to a positive value of dT_c/dp. As noticed by Samara,[44] the rare-earth pentaphosphates do not follow the same rule as most of the displacive ferroelectric crystals whose transition is induced by a zone-Brillouin-center soft optic mode for which $dT_c/dp < 0$.

Secondly, the pressure dependence of the soft-mode frequency ω_Q is then given by

$$\frac{d \ln \omega_Q}{dp} = -\frac{1}{2\omega_Q} \frac{d\omega_Q^2}{dT} \frac{dT_c}{dp} \quad . \tag{13}$$

We find $d \ln \omega_Q/dp \approx 11.64\%$ kbar^{-1} at $T_c - 49\,^{\circ}$C while Peercy's measurements[28] in TbP_5O_{14} give 11.08%.

Therefore, the set of these experimental data clearly shows that the phenomenological model used to explain the properties of LaP_5O_{14} can be extended to all the ferroelastic ReP_5O_{14} compounds qualitatively as well as quantitatively with close values of all the parameters of Eq. (8), except T_0, in all these materials.

However, two features of the considered transitions are not accounted for by the present model. In the first place, the experimental ratio of the slopes of ω_Q^2 on either side of T_c is 4.80 ± 0.25 significantly different from that relative to c_{55} (2.90), while both numbers are expected to be equal. However, this equality relies on the assumption of only one bilinear coupling term $\gamma e_5 Q$ in the expansion. It is easy to check that the introduction of higher-order coupling terms in the expansion such as $\lambda e_5^2 Q^2$ leading to a renormalized temperature-dependent γ coefficient in Eq. (9) will predict distinct slopes ratios[45] for ω_Q^2 and c_{55}. Considering the strength of the linear coupling, which is disclosed by the large shift $(T_c - T_0)$, we can understand that these higher-order coupling terms can contribute significantly to the results.

On the other hand, the c_{44} elastic constant is predicted to be unaffected by the transition while a slight anomaly has been observed at T_c (Fig. 8). It can be understood if we remember the existence of a second soft optic mode[21,22] of the same B_{3g} symmetry as the strain e_4. Thus, this mode which was not included in the free-energy expansion can linearly couple with e_4 as the B_{2g} soft optic mode couples with e_5. Here again, the softening of the B_{3g} mode on both sides of T_c induces the anomaly of the c_{44} temperature dependence since we have

$$c_{44} = c_{44}^0 - \gamma'^2/m'\omega'^2 \tag{14}$$

in both phases by analogy with Eq. (9), where γ' is the coupling coefficient between e_4 and the B_{3g} mode of mass m' and frequency ω'. Thus, we can fit the temperature dependence of c_{44} with ω' being determined by previous Raman-scattering measurements,[21] $c_{44}^0 = 3.15 \times 10^8$ and $\gamma'^2/m' = 8.15 \times 10^{12}$ which is nearly 3 times smaller than the coupling coefficient between Q and e_5 ($\gamma^2/m = 26.5 \times 10^{12}$). This fit is plotted with a dashed line below T_c in Fig. 8.

V. CONCLUSION

In this paper, we have presented an experimental and phenomenological study of the mechanical and elastic properties of ferroelastic lanthanum pentaphosphate. The set of thermal-strain and elastic-stiffness-tensor components as well as the sound velocities along the crystallographic axes and the bisectors of these axes have been determined on both sides of the $T_c = 125\,^{\circ}$C transition temperature. The continuity of all these quantities, mainly of the spontaneous shear, and the lack of thermal hysteresis confirm the second-order character of the transition while the influence of the fluctuations near the transition was found to be negligible as shown by the classical values of the critical exponents ($\beta = 0.500 \pm 0.007$ and $\gamma = 1.00 \pm 0.02$) related to e_5 and c_{55}.

As a consequence, in agreement with the Cowley and Schwabl renormalization-group calculation, we have shown that the ferroelastic transition of rare-earth pentaphosphates could be quantitatively explained by the mean-field Landau theory even in the vicinity of T_c. The set of available experimental results on these compounds: the temperature dependence of the thermal-strain and elastic-stiffness-tensor components in both phases, and of the B_{2g} soft-mode frequency above T_c, the pressure effect on this frequency as well as the jump of the specific heat have been fitted with a good accuracy (from 0 to 8%) by making use of a Landau free-energy expansion with only four coupling coefficients between the normal coordinate Q of the B_{2g} soft optic mode taken as the primary order parameter of the transition and the components of the strain tensor. It is worth noting that both static measurements (γ-ray and mechanical dilatometry, specific-heat) and dynamical ones (Raman and Brillouin scattering) are well accounted for by the same coupling coefficients, showing that no relaxation processes occur in the frequency range of all the experiments performed.

Q is quadratically coupled with the diagonal components of the strain tensor, but the main feature of the model is the strong bilinear coupling between Q and the monoclinic shear e_5, which is responsible for the destabilization of a transverse-acoustic mode. As a consequence, the ferroelastic transition occurs at T_c, 161 °C above the temperature T_0 where the frequency of the soft optic mode would vanish in the absence of the coupling. Such a strong coupling has already been observed in other materials undergoing a second-order proper ferroelastic transition such as $KH_3(SeO_3)_2$ (Ref. 13) ($T_c - T_0 = 137\,^{\circ}$C) or $BiVO_4$ (Ref. 46) ($T_c - T_0 = 228\,^{\circ}$C).

It would be interesting to identify the origin of this strong coupling at a microscopic level. In this aspect, structural data have shown that ferroelastic ReP_5O_{14} are formed by PO_4 tetrahedra sharing corners to produce parallel chains.[47] As pointed out previously,[25] the soft B_{2g} optic mode should correspond to a rotation of the tetrahedra. An examination of the structure[45] suggests that, because of bonding conditions between these tetrahedra, the rotation is correlated with a relative translation between the chains which induces the monoclinic strain of the unit cell. A more detailed study of this coupling is in progress.

ACKNOWLEDGMENTS

I would like to thank J. C. Toledano for constant advice during the course of this study as well as for a critical reading of the manuscript. γ-ray-diffractometry measurements were performed on LI3 at the Laue-Langevin Institut with the kind help of P. Bastie. It is also a pleasure to thank H. Savary for his expert growing of the crystals used in this study and G. Le Roux, R. Bertrand, and J. Brandon for orienting and polishing of the samples.

[1]J. C. Toledano, Ann. Télécomm. 29, 249 (1974).
[2]V. Dvořak, Ferroelectrics 7, 1 (1974).
[3]K. Aizu, J. Phys. Chem. Solids 32, 1959 (1971).
[4]W. Rehwald, Adv. Phys. 22, 721 (1973).
[5]L. D. Landau and E. Lifschitz, *Statistical Physics* (Addison-Wesley, Reading, Mass., 1958).
[6]N. Boccara, *Symétries Brisées* (Hermann, Paris, 1976).
[7]R. A. Cowley, Phys. Rev. B 13, 4877 (1976); F. Schwabl, Z. Phys. B 25, 69 (1976).
[8]H. Schulz, K. H. Thiemann, and J. Fenner, Mater. Res. Bull. 9, 1525 (1974).
[9]H. P. Weber, B. C. Tofield, and P. F. Liao, Phys. Rev. B 11, 1152 (1975); J. P. Budin, A. Milatos Roufos, N. Duch Chinh, and G. Le Roux, J. Appl. Phys. 46, 2867 (1975).
[10]T. Kobayashi, T. Sawada, H. Ikeo, K. Muto, and J. Kai, J. Phys. Soc. Jpn. 40, 595 (1975).
[11]J. Sivardière, Phys. Rev. B 6, 4284 (1972).
[12]F. Jona and G. Shirane, *Ferroelectric Crystals* (Pergamon, New York, 1962), p. 351.
[13]Y. Makita, F. Sakurai, T. Osaka, and I. Tatsuzaki, J. Phys. Soc. Jpn. 42, 518 (1977).
[14]P. S. Peercy and I. J. Fritz, Phys. Rev. Lett. 32, 466 (1974).
[15]H. G. Danielmeyer and H. P. Weber, IEEE J. Quantum Electron. QE8, 805 (1972).
[16]B. C. Tofield, P. M. Bridenbaugh, and H. P. Weber, Mater. Res. Bull. 10, 1091 (1975).
[17]J. P. Budin, M. Neubauer, and M. Rondot, IEEE J. Quantum Electron. QE14, 831 (1978).
[18]J. C. Toledano, G. Errandonea, and J. P. Jaguin, Solid State Commun. 20, 905 (1976).
[19]P. S. Peercy, in *Proceedings of the Fifth International Conference on Raman Spectroscopy, Freiburg, 1976* (Heyden & Sons), p. 571.
[20]D. L. Fox, J. F. Scott, and P. M. Bridenbaugh, Solid State Commun. 18, 111 (1976).
[21]G. Errandonea and J. Sapriel, Solid State Commun. 32, 391 (1979).
[22]W. K. Unger, Solid State Commun. 29, 601 (1979).
[23]D. L. Fox, J. F. Scott, P. M. Bridenbaugh, and J. W. Pierce, J. Raman Spectros. 7, 41 (1978).
[24]P. B. Miller and J. D. Axe, Phys. Rev. 163, 924 (1967).
[25]J. F. Scott, Ferroelectrics 20, 69 (1978).
[26]J. Fousek, C. Konak, and G. Errandonea, J. Phys. C 12, 3197 (1979).
[27]G. M. Loiacono, M. Delfino, and W. A. Smith, Appl. Phys. Lett. 32, 595 (1978).
[28]P. S. Peercy, J. F. Scott, and P. M. Bridenbaugh, Bull. Am. Phys. Soc. 21, 337 (1976).
[29]M. Marais, N. Duc Chinh, H. Savary, and J. P. Budin, J. Cryst. Growth 35, 329 (1976).
[30]J. F. Nye, *Physical Properties of Crystals* (Oxford University Press, New York, 1972).
[31]J. R. Schneider, J. Appl. Crystallogr. 7, 541 (1974).
[32]H. Z. Cummins, *Light Scattering in Solids* (Flammarion, Paris, 1971).
[33]J. R. Sandercock, *Light Scattering in Solids* (Flammarion, Paris, 1971).
[34]J. C. Toledano and M. Busch, J. Phys. (Paris) Lett. 36, L-141 (1975).
[35]R. Vacher and L. Boyer, Phys. Rev. B 6, 639 (1970).
[36]P. Bastie, J. Bornarel, J. Lajzerowicz, M. Vallade, and J. R. Schneider, Phys. Rev. B 12, 5112 (1975).
[37]S. Aubry and R. Pick, J. Phys. (Paris) 32, 657 (1971).
[38]G. A. Smolenskii and Z. M. Hashkozev, Mater. Res. Bull. 6, 1065 (1971).
[39]Cao Xuan An, G. Hauret, and J. P. Chapelle, C. R. Acad. Sci. 280, 543 (1975).
[40]S. I. Chizhikov, N. G. Sonokin, B. I. Ostrovskii, and V. A. Meleshina, Zh. Eksp. Teor. Fiz. 14, 490 (1971) [Sov. Phys. JETP 14, 336 (1976)].
[41]Cao Xuan An, G. Hauret, and J. P. Chapelle, Solid State Commun. 24, 443 (1977).
[42]E. M. Brody and H. Z. Cummins, Phys. Rev. Lett. 21, 1263 (1968).
[43]P. A. Fleury, J. Acous. Soc. Amer. 49, 1041 (1971).
[44]G. A. Samara, Comments Solid State Phys. 8, 13 (1977).
[45]G. Errandonea (private communication at the 4th European Meeting on Ferroelectricity) [Ferroelectrics (to be published)].
[46]A. Pinczuk and F. H. Dacol, Solid State Commun. 29, 515 (1979).
[47]H. Y. P. Hong, Acta Crystallogr. Sect. B 30, 468 (1974).